CELL-INSTRUCTIVE MEMBRANE BIOMATERIAL FOR NON-UNION BONE HEALING

Efrén Miguel Rojas Moreno

ATLAS Bachelor's Thesis

In Collaboration with the Molecular Nanofabrication (MNF)

Faculty of the University of Twente

June 2024

Table of Contents

Abstract **1**

List of Abbreviations **1**

1. Introduction **2**
1.1 Non-Union Bone Fractures 2
1.2 Actors and Mechanisms Involved in Bone Growth and Healing 3
1.3 Enhancing Bone Regeneration through P-15 Peptide Integration 4
1.4 Functionalised Synthetic Membrane for Non-Union Fracture Treatment 5

2. Scope of the project **6**

3. Methodology **6**
3.1 Native PET Mesh Preparation 6
3.2 Functionalisation of PET Meshes with P15 Peptide 6
3.3 Contact Angle Measurements 7
3.4 Human Osteoblast Cell Culture and Cell Experiments 8
3.5 Immunofluorescence Procedure 8

4. Results **10**
4.1 PET Membrane Functionalisation 10
4.2 Human Osteoblast Cell Immunofluorescence 11
4.3 HOBs on Meshes Experimental Immunofluorescence Analysis 13

5. Discussion **16**

6. Conclusion **17**

7. Works Cited **18**

Appendix A: Contextual Exploration **21**

Appendix B: Reaction Mechanism **23**

Appendix C: Additional Immunofluorescence Imaging Results **24**

Appendix D: HOBs in Cell Culture Brightfield Microscopy Imaging **29**

Abstract

Enhancing the healing of non-union bone fractures is a critical challenge in orthopaedic medicine, necessitating the development of advanced biomaterials. This study investigates the efficacy of P15 peptide-functionalised polyethylene terephthalate (PET) membranes in promoting osteogenic differentiation and bone regeneration. The PET membranes were treated to attach P15 peptides using oxygen plasma, NaOH, and EDC/NHS coupling, with successful functionalisation confirmed via contact angle measurements. Human osteoblast cells (hOBs) were then cultured on native, Collagen I-coated, and P15-treated membranes, and their interactions were analysed through immunofluorescence staining and confocal microscopy to assess integrin expression, focal adhesion formation, and cell morphology. Results demonstrated that P15-functionalised PET membranes indicate potential for good cell adhesion, integrin localisation, and focal adhesion formation, suggesting a conducive environment for osteogenic activity. These findings indicate that P15-functionalised PET membranes hold promise for enhancing bone regeneration in non-union fractures, supporting their potential application in clinical orthopaedic treatments.

List of Abbreviations

αMEM	α Minimum essential medium
BSA	Bovine serum albumin
DNA	Deoxyribonucleic acid
ECM	Extracellular matrix
EDC	1-Ethyl-3-(3-dimethylaminopropyl)carbodiimide
FAK	Focal adhesion kinase
FBS	Foetal bovine serum
HOB	Human osteoblast
MES	2-(N-morpholino)ethanesulfonic acid
MQ	Milli-Q
NHS	N-Hydroxysuccinimide
OPT	Oxygen Plasma Treatment
P/S	Penicillin/streptomycin
PBS	Phosphate-buffered saline
PFA	Paraformaldehyde
PET	Polyethylene terephthalate
TEP	Tissue-engineered periosteum
TX	Triton X-100

1. Introduction

1.1 Non-Union Bone Fractures

Non-union fractures pose a considerable challenge in orthopaedic medicine, occurring when a fractured bone fails to heal properly [1]. This failure can be attributed to various factors such as inadequate immobilisation, unsuccessful surgical intervention, insufficient biological response, or infection, resulting in prolonged periods without healing [1]. It manifests as a chronic medical condition characterised by persistent pain and functional limitations, leading to substantial psychosocial disability [1]. Diagnosis typically involves plain X-ray imaging, often supplemented by computer tomography scans to define anatomical details, especially in complex cases [1]. Symptoms include persistent pain, deformity, and poor limb function, along with signs of infection or failed prior surgery [1]. The risk of developing non-union varies worldwide, ranging from 1.9% to 4.9%, with profound physical and psychosocial impacts on affected individuals [1].

Understanding the mechanisms and pathophysiology of non-union fractures is crucial for developing effective treatment strategies [1]. Successful bone healing relies on adequate alignment and stabilisation of bone fragments to minimise fracture gap size and interfragmentary movement [1]. This process involves a complex interplay of cytokines, chemokines, and growth factors, such as TGFβ, BMPs, Wnt–β-catenin, and VEGF that activate signalling pathways facilitating cell migration, proliferation, and differentiation [1]. Bone remodelling, orchestrated by bone-forming osteoblasts and bone-resorbing osteoclasts, is crucial for renewal, repair, and adaptation to mechanical requirements throughout life [1]. Non-union fracture healing processes can also be categorised into primary and secondary bone healing, where the stage is dependent on certain factors such as bone fragment distance, mechanical conditions, and anatomical location [1]. Primary bone healing occurs under rigid fixation, whereas secondary bone healing involves the formation of an external callus due to interfragmentary movement, followed by overlapping phases of inflammation, repair, and remodelling [1].

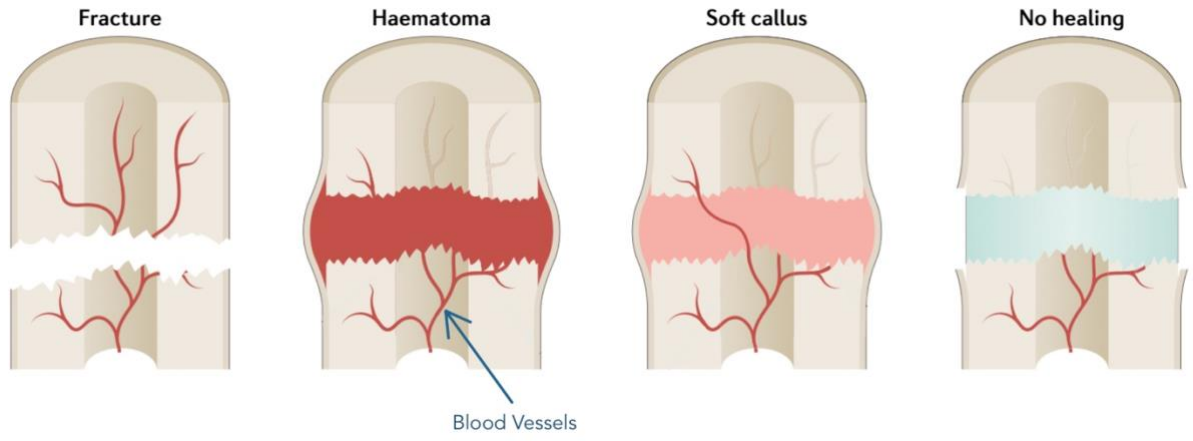

Figure 1. Phases of non-union formation (adapted from [1]). *Following a fracture, the afflicted zone (haematoma) becomes inflamed, which sets off an immunological reaction and creates a fibrin clot that serves as a scaffold [1]. The cartilaginous and fibrous tissue then creates a soft callus, which later hardens into a bony callus and finally reshapes the bone [1]. This bone repair process can be affected through changes in the biological environment or mechanical instability, though, ultimately leading to non-union [1].*

Current medical treatment approaches for non-union fractures involve addressing both patient-dependent and independent risk factors [1,2]. These include modifiable factors like smoking, alcohol consumption, nutritional deficiencies, and high body mass index, as well as non-modifiable factors such as age, gender, and genetic predisposition [1,2]. Surgical interventions aim to promote bone regeneration and healing, with considerations for factors under the surgeon's control, such as choice of surgery, stabilisation techniques, and follow-up protocols [1,2].

Several biomaterials-based strategies have also come to light as viable treatments for non-union fractures of the bone [15]. With the benefits of autografts and allografts avoided, synthetic bone transplants are designed to resemble natural bone characteristics and aid in healing [15, 16]. Because mesenchymal stem cells create an environment that is favourable for differentiation and bone creation, stem cell therapy can also improve bone regeneration [17]. Injectable stem cell gels and scaffold-based stem cell administration are two techniques for minimally invasive therapy [17]. Furthermore, adding growth factors to biomaterial scaffolds, such as platelet-rich plasma and bone morphogenetic proteins, can dramatically improve bone repair. These elements are useful in the treatment of non-union fractures because they promote the growth of new bone and tissue [17].

1.2 Actors and Mechanisms Involved in Bone Growth and Healing

The periosteum, an integral tissue in bone repair, provides essential blood supply and cellular components necessary for healing [3]. It is a two-layered membrane made up of an inner layer rich in osteogenic cells and an outer layer made of fibrous tissue that covers the outer surface of bones [3]. It offers a location for bone growth and regeneration, shields bones from mechanical harm, and acts as a point of attachment for tendons and ligaments [3]. It acts as a natural reservoir of many signalling molecules that promote bone regeneration [3]. Rapid periosteal responses following injury underscore its significance in the bone healing process, with its involvement often associated with endochondral ossification [3]. The biochemical properties of the periosteum significantly contribute to fracture prevention by enhancing cortical bone strength through periosteal expansion, independent of changes in areal bone mineral density [20].

The periosteum structurally exhibits distinct mechanical and chemical properties, with stem cells in its inner layer particularly sensitive to external stimuli, influencing cell behaviour and fate [3]. Consequently, the modification of mechanical properties, such as matrix stiffness, and surface topography becomes crucial in tissue-engineered periosteum (TEP) design, ensuring optimal bone regeneration and integration [3]. In recent years, tissue-engineered periosteum (TEP) has emerged as promising avenues for enhancing bone regeneration [3]. TEP grafts, developed using natural or synthetic materials, aim to harness the advantages of periosteum to promote bone regeneration therapies [3].

The extracellular matrix (ECM) is heavily involved in bone regeneration, providing mechanical support, and regulating cell behaviour [3]. Naturally, tissue-derived ECM scaffolds offer promising materials for tissue engineering, promoting bone regeneration in various animal models [3]. An alternative approach to this one is that of cell-derived ECMs and peptides that mimic the proteins involved. These are relevant since cells are cultured to secrete and deposit ECM components, forming a scaffold mimicking natural tissue ECM [3]. The peptides involved, which are much smaller in size than full proteins and are thus much easier to synthesise, offer a simple solution that fulfils the basic target ECM and experimental functions

[19]. They can be conjugated to biomaterials with great precision using procedures like amine/19ylic acid coupling, resulting in a heterogeneous mixture of conformations of attached protein [19]. Historically, these have demonstrated great potential in promoting cell proliferation, osteogenic potential, and angiogenic capacity, making them suitable for periosteum tissue engineering [3].

Signalling molecules such as the cytokines, chemokines, and growth factors mentioned above are often sequestered within the ECM or bound to ECM components, where they act as reservoirs or undergo regulated release [3]. Additionally, the ECM can modulate the activity and availability of these molecules, influencing cell behaviour and function [3].

1.3 Enhancing Bone Regeneration through P-15 Peptide Integration

As a synthetic sequence of 15 amino acids, the P15 peptide plays a pivotal role in enhancing bone regeneration through its unique mechanism of action [8]. P15 mimics a specific cell-binding domain found in type I collagen, a fundamental organic component of bone tissue, and thus demonstrates remarkable capabilities in promoting cell attachment, migration, proliferation, and differentiation [8,10]. The presence of the aforementioned cell-binding domain of collagen I allows P15 to be adsorbed onto a calcium phosphate substrate, which in turn and results in bone formation [8].

At a molecular level, P15 functions by simulating a distinct biochemical property of cellular environment, facilitating interactions between cells and ECM elements [13]. Due to its great similarities to collagen I, P15 can bind to cell-surface integrin receptors, specifically α2B1 integrins, which then initiates activation of focal adhesion kinases (FAK) [20]. FAKs are important mediators of signal transduction pathways involved in cell migration, survival, and differentiation, and their activity can be monitored with immunofluorescence techniques [20]. This all makes P15 an effective mimic of bone extracellular matrix for promoting bone repair processes [8,10].

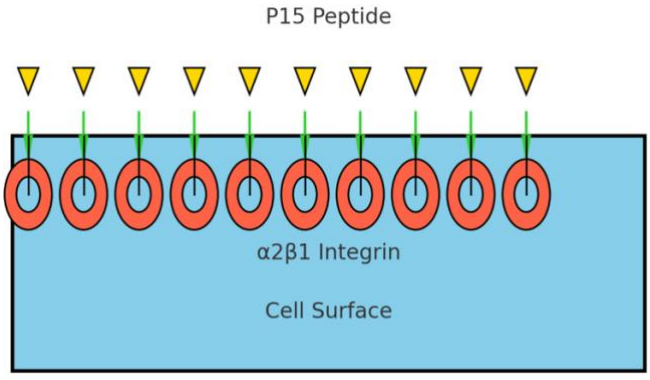

Figure 2. Interaction between P15 Peptides and α2β1 Integrins on the Cell Surface. *The cell surface is represented as a blue rectangular area, providing the structural foundation for integrin receptors [20]. Above this surface, yellow triangular structures depict the P15 peptides. Embedded within the surface are the α2β1 integrin receptors, shown as red circular structures, which play a crucial role in cell adhesion and signalling processes [20]. Green arrows indicate the specific binding interactions between the P15 peptides and the α2β1 integrins.*

In clinical applications, P15 has emerged as a safe, economical, and clinically useful alternative to autografts in the treatment of non-unions and delayed unions [8]. The P15 bone graft substitute has shown efficacy in facilitating the repair of ununited fractures by enhancing cell attachment, migration, and proliferation in the bone repair process [8, 13].

Furthermore, the integration of P15 with biomaterials, such as polyethylene terephthalate (PET) membrane meshes (with defined pore sizes), offers a promising avenue for mimicking periosteal conditions and enhancing bone regeneration processes [13]. Covalently attaching P15 to biomaterials can promote cell-derived ECM formation and cellular activity, providing a conducive environment for bone tissue regeneration [8, 13]. This integration allows for the localisation of migrating bone cells and acts as a barrier to prevent cell migration beyond the membrane, which is further controlled by the small membrane pore size (5um) relative to cellular dimensions, ensuring localised cellular activity for effective bone repair [13].

1.4 Functionalised Synthetic Membrane for Non-Union Fracture Treatment

Due to the finite availability of periosteum, there is a requirement for biomaterial-based approaches to develop durable implants mimicking the properties of periosteum. However, existing biomaterial strategies often suffer from inadequate mechanical strength and stability or rely on animal-derived components lacking clinical suitability, limited bioactivity, and insufficient control over multiple cell-instructive signals [3, 12]. Hence, there is a pressing need to innovate novel biomaterials that replicate the characteristics of periosteum more accurately, offering improved control over their biological properties [12].

PET is widely used in medical applications due to its exceptional mechanical strength, durability, and biocompatibility, making it suitable for load-bearing applications like vascular grafts and surgical meshes [4, 21]. Its high resistance to chemicals and biological fluids ensures long-term structural integrity, crucial for consistent performance and safety in medical settings [22]. Moreover, PET can be fabricated in various forms, such as fibres and woven meshes, allowing for customised synthetic membranes tailored to specific applications, enhancing their functionality [23]. For instance, it can be treated with oxygen plasma, as is done in this research, to create carboxylic acid groups at the surface, essentially serving as the initial step for functionalisation, and are suitable for immunofluorescence protocols [19, 35]. Additionally, PET is non-toxic, does not release harmful substances, and has a proven clinical track record, providing confidence in its reliability and safety [4, 5]. Its cost-effectiveness and established manufacturing processes further make it an attractive option for developing affordable medical devices [6]. These attributes collectively support PET's continued use as a biomaterial and ongoing research into novel medical devices and implants.

Thus, the idea behind implementing PET membrane meshes is to mimic the role of the periosteum tissue, where post-biofunctionalisation, they should be able to undergo all processes detailed in the previous section. Due to its hydrophobic properties, the PET membrane must first be functionalised to allow for biocompatibility, after which further proteins and molecules can then be covalently attached to the membrane to promote bone regeneration processes [8]. Moreover, PET has been noted to be suitable for fluorescence imaging, which introduces advantages when analysing cell-material interactions, especially in terms of integrin localisation and focal adhesion formation studies, as are targeted in this project [9].

2. Scope of the project

The focus of this thesis project is to investigate the behaviour of hOBs on PET membrane biomaterials that are functionalised with P15 peptide that is known to induce specific bone cell-adhesion and biological processes involved in bone differentiation, If effective, this technique could prove to be a significant step towards the development of novel bone cell-instructive, periosteum-mimetic biomaterial, targeted for the improvement of bone formation and achieving full regeneration from non-union fractures. Thus, the driving, overarching question for this research project can be formulated in the following way:

To what extent is a P15-treated PET membrane functional in regard to human-derived bone cell activity and enhancement of non-union fracture healing?

Initially, the focus will lie on analysing the integrin subtypes engaged in osteogenic differentiation and their interactions with Collagen I and Collagen I-derived peptides (P15) in human bone cells sourced from VU collaborators. Through meticulous analysis on Collagen I and fibronectin coated glass substrates, the study will seek to identify Beta 1 integrin expression/localisation, focal adhesion formation, and cell morphology, employing techniques such as immunofluorescence, confocal imaging, and multiplexed imaging via antibody staining. In principle, the procedure for functionalising the PET membrane meshes (PET woven mesh: 2% open area, 5 μm pore size, 65 μm thickness; Repligen, USA) to promote peptide attachment will be based on a study made prior to this one [14]. The procedures that follow consist of a combination of techniques that have been cross-checked with literature online.

Subsequently, the attention will shift towards the evaluation of cell-material interactions on P15-functionalised membrane meshes, with a primary focus on the mechanisms underlying integrin-mediated adhesions and cellular morphology amidst the presence of osteogenic peptides/factors (primarily P15 peptide). Conditions will comprise PET membrane meshes functionalised with P15 peptide, Collagen I-coated and oxygen plasma-treated PET, and non-treated native mesh. These biomaterial surfaces will be investigated for specific integrin expression/localisation, focal adhesion formation, and overall cell morphology analyses.

3. Methodology

3.1 Native PET Mesh Preparation

The PET membranes were cut and punched on the bottom right corner (1.0-1.5 x 1.0-1.5 cm), and then cleaned by successive washes in MilliQ-ethanol absolute-MilliQ (by shaking at 250 rpm for 5 min in 40mL of each solution). They were then air dried using a nitrogen gun and stored individually in each well of a 12 well polystyrene plate.

3.2 Functionalisation of PET Meshes with P15 Peptide

The functionalisation of the PET meshes consisted of several steps after which contact angle measurements were drawn to verify the success of the procedure. The prepared meshes were treated through an oxygen plasma treatment (OPT) at 40 mbar for 20s at 40% power, after which they were immediately submerged in 1M NaOH and shaked for 1hr at 150rpm, to introduce functional groups such as hydroxyl, carboxyl, and carbonyl groups. Next, they were washed (2mL MilliQ, 10min at 150rpm 2X), treated with 50mM of EDC (1-Ethyl-3-(3-dimethylaminopropyl) carbodiimide) and NHS (N-hydroxysuccinimide) in a 2mL MES buffer

solution (100mM of MES at pH of 5.2, shaked in glass vials for 1hr at 150rpm), and washed 2X more in MilliQ. This results in the formation of an activated ester that is highly reactive towards nucleophiles, such as amines, thus preparing it for peptide coupling [30].

Upon this treatment, the meshes were then moved into vials containing 1mM P15 of peptide in 1.5mL of phosphate buffered saline (PBS, at a pH of 7.45) and shaked in glass vials for 2h at 150rpm before being washed 2X in MilliQ. The resulting meshes with covalently attached peptides were then dried with a nitrogen gun and stored under Argon in a nitrogen-controlled environment, to preserve the peptide's conditions as best as possible. This procedure for peptide coupling was followed from Thermo-Scientific's procedure for solid-phase immobilisation applications (reaction mechanism in Appendix B) [11].

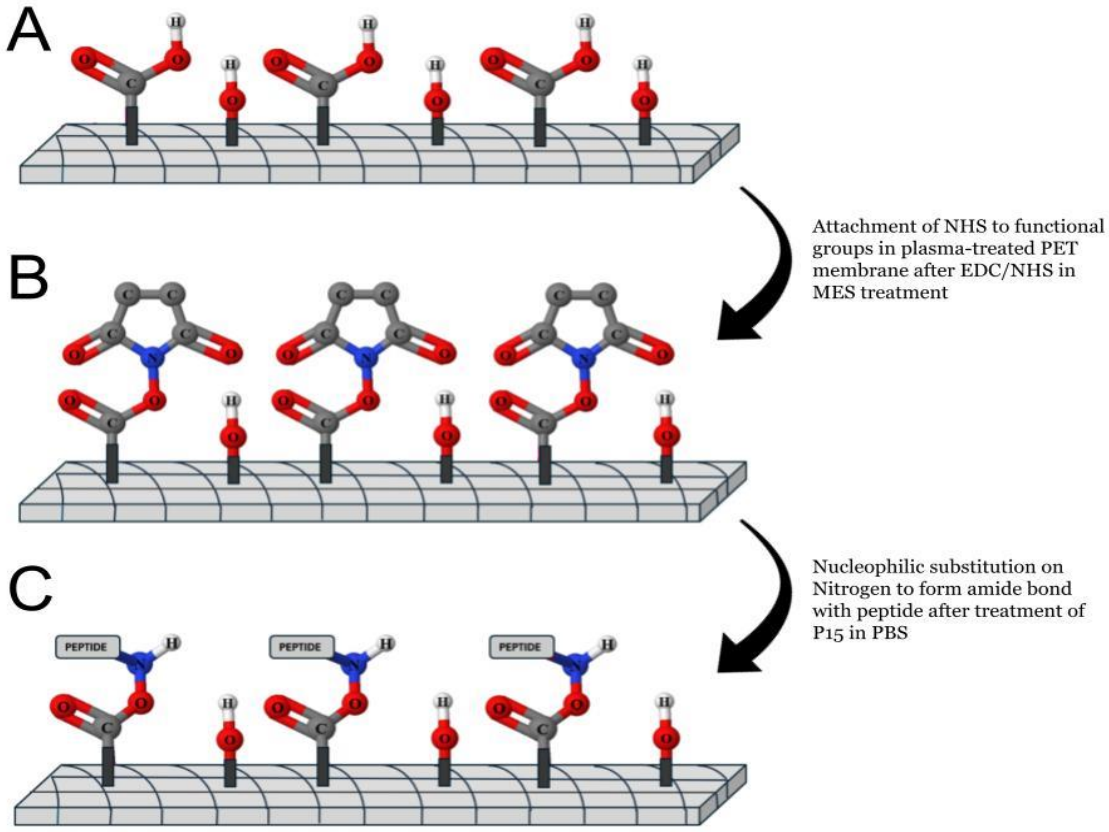

Figure 3. Diagram outlining the process for functionalising the surface of the PET membrane with the P15 peptide (adapted from [14]).

A. The PET surface, treated with OPT and NaOH, presents functional groups.
B. EDC/NHS treatment is applied for the formation of an NHS intermediate connected to the PET surface.
C. PET surface is functionalised with peptide after P15-treatment.

3.3 Contact Angle Measurements

To ensure the robustness of the procedure and verify appropriate completion of all steps, water droplet contact angles (CA) were regularly checked with a drop shape analyser DSA30S (Krüss, Germany). This returned information on the hydrophilicity of the meshes, which were subject to change as a result of the different treatments received. The meshes were individually placed in the machine, and a 2um droplet was produced from a syringe, which was then set on top of

the sample. The time taken for the mesh to fully absorb the droplet, and the angle formed between the edges of the droplet and the mesh were recorded after 15 seconds.

3.4 Human Osteoblast Cell Culture and Cell Experiments

Human osteoblasts were isolated from healthy bone tissues by collaborators at UTwente (tissues are supplied from ACTA/Amsterdam UMC, Vrije Universiteit). Cells are cultured in minimum essential medium α (αMEM; [+] Ribonucleosides, [+] Deoxyribonucleosides) with 10% foetal bovine serum (FBS) and 1 % penicillin/streptomycin (P/S), up to passage 5. A maximum of three days was allowed for cells to remain in culture medium before being placed in fresh medium.

For cell experiments, the following procedure was followed. First, meshes were prepared in OPT. These meshes were then maintained in Milli-Q (MQ) water while moving to the cell lab, after which they were transferred into a sterile well plate containing PBS (2mL per well). For the preparation of the Collagen I solution, the solution was prepared on ice to prevent gelling. 160µL of Collagen I was mixed with 7.84mL of 20mM Acetic Acid (23µL of Acetic Acid in 20mL of MQ). Two meshes were then transferred from the PBS to the Collagen I solution and incubated for 1 hour, followed by washing them with PBS three times.

12 mL of normal medium (5mL to block trypsin and 5 mL for passaging) and 15mL of serum-free medium (αMEM + 1% P/S) were then prepared and warmed up for use with the six meshes (2X P15-treated, 2X OPT+Collagen I-treated, and 2X Native), two Collagen I coated suspension wells, and two non-coated suspension wells (1.5mL of medium per well). Next, cells were trypsinised and counted: The medium was removed, and 5 mL of PBS was added to wash the cells. After this, 1mL of trypsin was added and the cells were incubated for a maximum of 5min, including 1-2min in the incubator. To neutralise the trypsin, 5mL of medium was added, and the cells were pipetted up and down to wash the surface. All cells were then transferred into a 50mL falcon tube and centrifuged at 1.1rpm for 5 minutes. The resulting cell pellet was resuspended in 1mL of serum-free medium.

Cell counting was performed in the new serum-free medium, ensuring the correct cell counting procedure was followed. A total of 175,000 cells were required (5,000 cells/cm2 hOBs seeding density → 17,500 cells/3.5cm2 wells, for 10 wells). Subsequently, 1.5mL of the cell suspension (cells + medium) was added to each of the 10 wells in the 12-well cell suspension plate. The 2X Collagen I treated meshes, 2X Native meshes, and 2X P15 meshes were transferred into six wells with the cell suspension and medium and incubated overnight. Additionally, 1.5 mL of serum-free medium was added to the two Collagen I-coated and two non-coated wells.

Finally, any remaining cells not used were resuspended with normal medium, and 5mL of this suspension was added to a T25 flask, which was then moved into the incubator for further culture.

3.5 Immunofluorescence Procedure

An established immunofluorescence procedure was used to stain the cells on the membranes [38]. After defined time points, cells were fixated with 4% paraformaldehyde (PFA) for 10 min, and washed 3X with PBS (10 min each). Samples or surfaces were stored at 4°C for immunofluorescence analysis or scanning electron microscopy measurements.

After fixation, the cells were permeabilised for 10 min in 0.5% Triton X-100 (TX) in PBS and then treated with a blocking solution of 0.1% TX and 5% bovine serum albumin (BSA) in PBS

for an hour. Afterwards, the meshes with cells were flipped and incubated onto 60uL droplets of a solution of AlexaFluor-647 phalloidin (1:100) and monoclonal anti-human vinculin-FITC antibody (1:200) in 0.1% TX and 5% BSA in PBS for 1h at room temperature, in the dark. The meshes with cells were then washed x3 with PBS before nuclear staining was performed using the same flipping technique with DAPI (1:1000) stains in PBS for 10 mins, and then finally washed x2 in PBS for 10 mins. Once again, the meshes with cells were covered and stored in a dark environment overnight at 4°C.

Zeiss 880 confocal microscope was used for imaging at 10x and 20x. Samples were placed on a petri plate with a droplet of PBS to prevent drying while measuring and loaded onto the machine. The 405, 488, and 633nm lasers were then selected for excitation of the fluorophores experimented with at 2-2.4% power each, and 1AU was selected as the pinhole size for each channel. The gain was manually modified to reduce background noise as much as possible in each case. For image acquisition, the nucleus of cells was initially targeted in using the 10x lens, after which the lens was switched to 20x and focused specifically on the nucleus.

Fixation, permeabilisation, and blocking are crucial steps in preparing cells and tissues for microscopy, each serving a distinct purpose to ensure accurate and detailed visualisation. Fixation preserves cellular structures by cross-linking proteins and other macromolecules, thereby stabilising the cells and maintaining their morphology, typically using agents like formaldehyde or glutaraldehyde [36, 37]. Permeabilisation, achieved using detergents such as Triton X-100, makes the cell membrane permeable, allowing stains and antibodies to access intracellular structures [36, 37]. Blocking is then employed to prevent non-specific binding of antibodies to cellular components, which is accomplished using proteins like BSA or normal serum, reducing background noise and enhancing the specificity of the signal [36, 37].

Staining hOBs with anti-human vinculin-FITC, phalloidin, and DAPI aims to analyse the cellular architecture, nuclear integrity, and focal adhesion dynamics in detail. A cytoskeletal protein called vinculin is linked to focal adhesions and cell-cell junctions. It is essential for the connection between integrins and the actin cytoskeleton, which helps to understand signalling cascades and cell adhesion [24]. Phalloidin binds exclusively to F-actin filaments to visualise the actin cytoskeleton, which is essential for preserving cell shape, permitting cell movement, and promoting intracellular transport [27]. Cell nuclei are stained with DAPI, a fluorescent dye that binds strongly to A-T rich areas in DNA and makes it easy to determine the number of cells and nuclear shape [28].

When combined, these stains allow for a comprehensive analysis of the spatial interactions among focal adhesions, the actin cytoskeleton, and cell nuclei. It is worth noting that while the presence of focal adhesions does suggest an extended cytoskeleton into that region, and vice versa, it does not guarantee that the cytoskeleton has fully extended onto that zone yet, for example [33, 34]. This improves our comprehension of the morphology and behaviour of hOBs under diverse experimental settings, including the impact of synthetic peptides like P15 on cytoskeletal organisation and cell adhesion.

Expected results include some of the following stains in the relevant cell component. In green, the stained vinculin focal adhesion kinases, which would provide insight on cell signalling, shape, and motility [24]. In red, the phalloidin dye would highlight the cell's cytoskeleton by staining F-Actin filaments, thus illustrating a clear cell shape and highlighting intercellular transport channels [27]. In blue, the DAPI-stained cell nucleus, which is used to determine

cell count and focusing for imaging [28]. The brightness and contrast of each image was then changed to the same respective values to improve visibility and reduce background noise.

4. Results

4.1 PET Membrane Functionalisation

These results focus on evaluating the changes in hydrophilicity of PET membranes following different surface modification treatments by measuring the contact angles of water droplets on the treated surfaces. Contact angle measurements provide crucial insights into the wettability and surface energy of the membranes, which directly impact their performance in different applications [27].

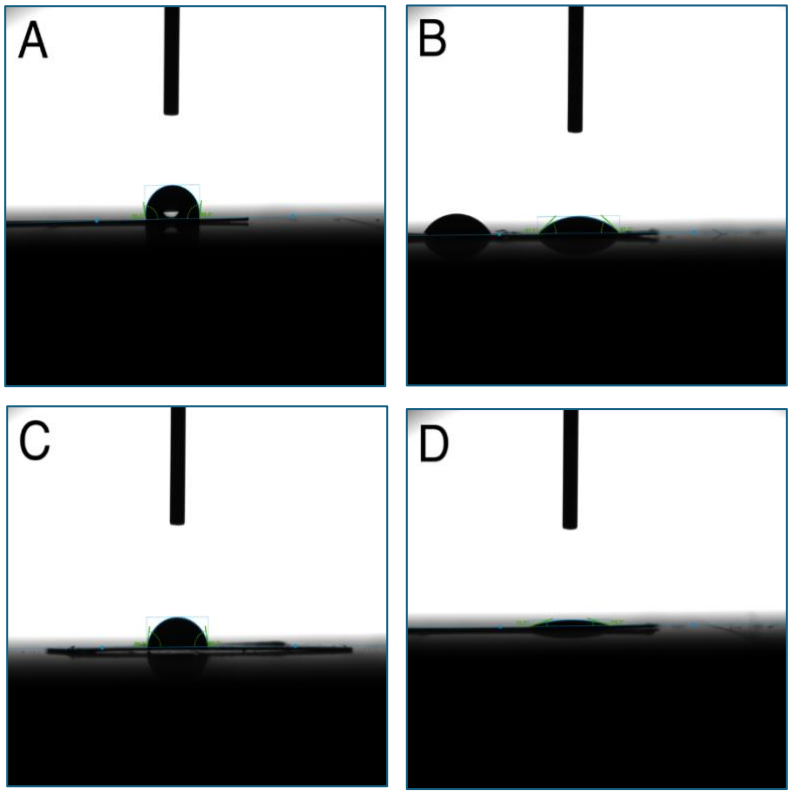

Figure 4: Contact angle between water drop and PET mesh after various membrane functionalisation treatments. *Images were taken 15 seconds after the drop was placed on the membrane, and a manual fit was then made to best approximate the contact angle.*

A. *Contact angle for native, untreated PET sample. Contact angles observed for native samples were in the 90°–100° range.*
B. *Contact angle for PET sample after Oxygen Plasma Treatment and Sodium Hydroxide treatment for 1h. Contact angles observed for OPT+NaOH treated samples were in the 25°–45° range.*
C. *Contact angle for PET sample after EDC/NHS treatment for 1h. Contact angles observed for EDC/NHS treated samples were in the 55°–80° range.*
D. *Contact angle for PET sample after P15 Peptide incubation for 2h. Contact angles observed for P15 treated samples were <20° and were frequently fully absorbed within 15-30 seconds.*

For the native sample, the high contact angle confirms that the untreated PET membrane has low surface energy, resulting in poor wettability. This is consistent with previous findings that native PET surfaces exhibit hydrophobic characteristics due to the lack of polar functional groups on the surface [27].

Next, the significant reduction in CA in image B of figure 4 indicates an increase in surface hydrophilicity, where OPT and NaOH likely introduced polar functional groups, such as hydroxyl and carboxyl groups, on the PET surface, which enhance its wettability [28].

Then, after EDC/NHS treatment, there is a moderate increase to the CA compared to the sample in the previous step. EDC and NHS are known to facilitate the attachment of hydrophilic groups to the PET surface, thus improving its wettability in relation to the native sample [30].

Finally, the substantial decrease in contact angle and the rapid absorption of water droplets indicate a highly hydrophilic surface. The peptide incubation likely resulted in significant surface modification, introducing highly polar or hydrophilic groups that enhance water uptake. Despite the lack of literature results available to either validate or reject these results, they do make sense, in theory. Using the Kyte-Doolittle scale and averaging the values of all the amino acids in the chain that makes up the P15 peptide (GTPGPQGIAGQRGVV) returns a value of -0.18, which initially suggests that the peptide should be mostly neutral [32]. However, P15 does have a much larger amount of hydrophilic amino acids that are close to each other, and other than the four amino acids in the chain with a large hydrophobicity, it is predominantly hydrophilic.

The purpose of the CA measurements was to confirm the successful completion of every step while gaining familiarity with the membrane functionalisation procedure, which was effectively validated by the results presented above.

4.2 Human Osteoblast Cell Immunofluorescence

Prior to experimentation of the cells on the meshes, it is necessary to see what the hOB cells looked like so to have a baseline for comparison afterwards. Figures 5 and 6 below show hOB cells that have been subjected to two different treatments (Collagen I and FBS, respectively), and their general morphology, focal adhesions and actin filaments can be observed.

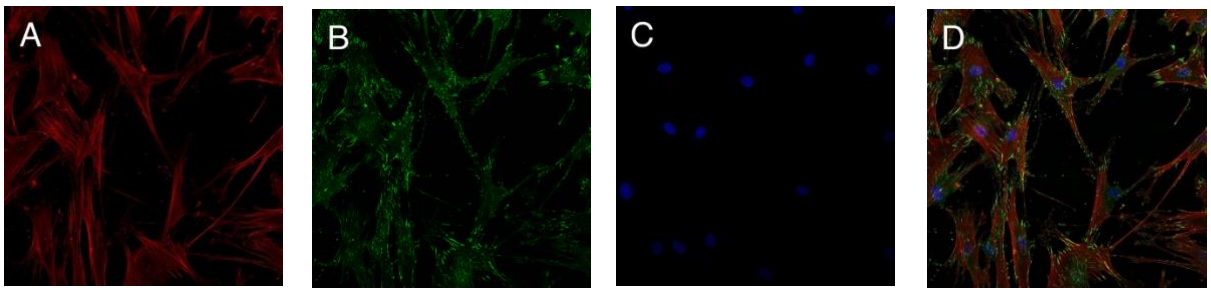

Figure 5: Confocal imaging and morphology of Collagen I coated human osteoblast cells. *Fixed cells were subjected to Vinculin, Phalloidin and DAPI staining, and images were acquired using 20x zoom Zeiss 880 confocal microscope for morphological analysis. Each image covers a dimension of 425µm x 425µm. The cells were seeded in 6 wells of a 96 well glass plate coated in Collagen I.*

A. Phalloidin staining of actin filaments.
B. Vinculin staining of focal adhesions.
C. DAPI staining of cell nuclei.
D. Composite image superposing Phalloidin, Vinculin, and DAPI staining to give holistic overview of control cell morphology characteristics.

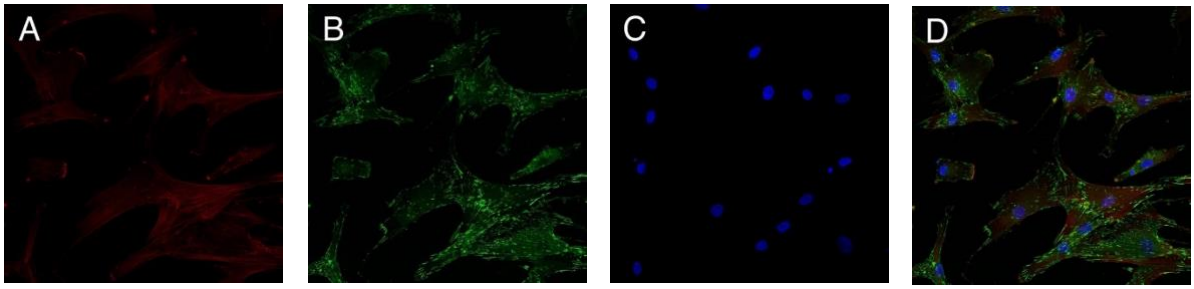

Figure 6: Confocal imaging and morphology of FBS-coated human osteoblast cells. *Fixed cells were subjected to Vinculin, Phalloidin and DAPI staining, and images were acquired using 20x zoom Zeiss 880 confocal microscope for morphological analysis. Each image covers a dimension of 425µm x 425µm. The cells were seeded in 6 wells of a 96 well glass plate coated in FBS.*

A. Phalloidin staining of actin filaments.
B. Vinculin staining of focal adhesions.
C. DAPI staining of cell nuclei.
D. Composite image superposing Phalloidin, Vinculin, and DAPI staining to give holistic overview of control cell morphology and characteristics.

The purpose of experimenting with different coatings on hOBs was to identify an optimal control sample for further comparative studies on cell characteristics when placed on meshes. The primary goal was to create an environment closely resembling the ECM to provide realistic conditions for bone cells. The study evaluated the cells' "comfort" and "well-being" by analysing characteristics such as their size, quantity, general shape, fluorescence signal intensity, and general morphology.

Comparative analysis of figures 5 and 6, along with additional confocal images presented in Appendix C.1, revealed that Collagen I-coated cells exhibited greater "comfort." This was indicated by the intensity and shape of the cytoskeleton, particularly the red-stained actin filaments. Collagen I-coated cells were more homogeneous and larger in size, whereas FBS-coated cells had more pointed physical characteristics and lower intensity. Additionally, the morphology of Collagen I-coated cells more closely matched literature-based expectations for cell structure in the ECM [31].

Therefore, Collagen I was determined to be the optimal baseline coating for further comparisons of functionalised meshes, as it best mimicked the conditions favourable for bone growth and healing.

4.3 HOBs on Meshes Experimental Immunofluorescence Analysis

After experimentation on the cells and confirming the expected morphology and physical characteristics of hOBs in the conditions of the experiment, testing proceeded on the actual meshes. Figures 7, 8, and 9 below show hOB cells that have been seeded on PET surfaces that have been subjected to different treatments (Native, OPT+PBS, and P15, respectively).

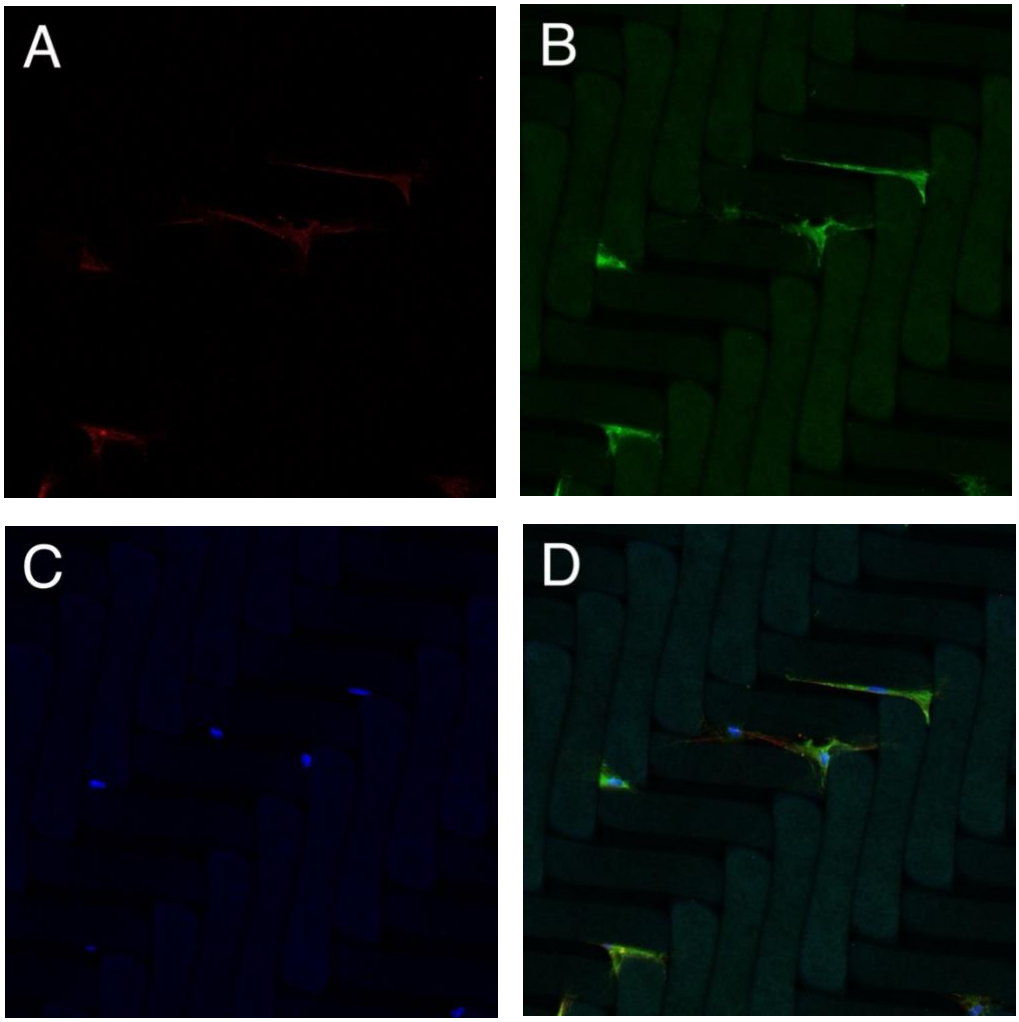

Figure 7: Confocal imaging and morphology of human osteoblast cells on a Native PET membrane. *Fixed cells were subjected to Vinculin, Phalloidin and DAPI staining, and images were acquired using 20x zoom Zeiss 880 confocal microscope for morphological analysis. Each image covers a dimension of 425µm x 425µm. The cells were placed in wells with untreated meshes.*

A. *Phalloidin staining of actin filaments.*
B. *Vinculin staining of focal adhesions.*
C. *DAPI staining of cell nuclei.*
D. *Composite image superposing Phalloidin, Vinculin, and DAPI staining to give holistic overview of control cell morphology characteristics.*

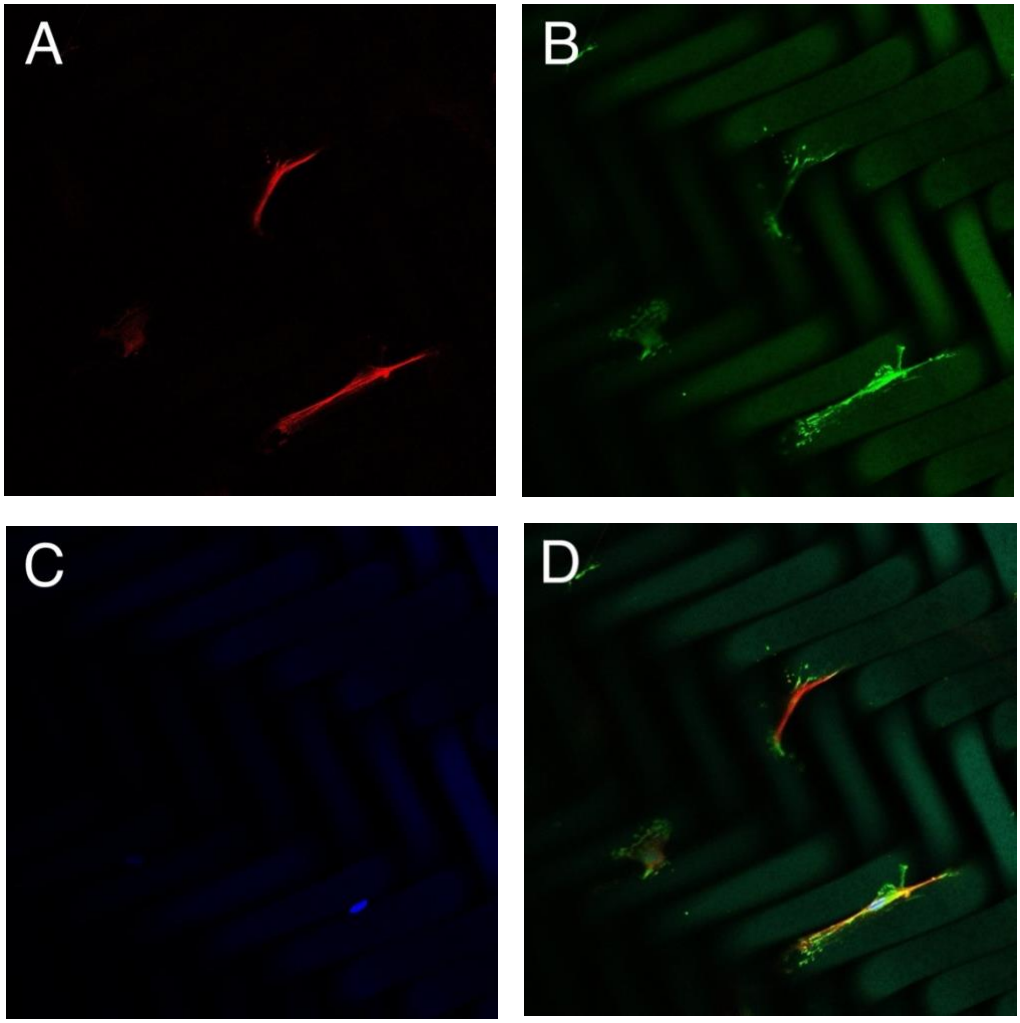

Figure 8: Confocal imaging and morphology of human osteoblast cells on a Collagen I coated and OPT+PBS treated PET membrane. *Fixed cells were subjected to Vinculin, Phalloidin and DAPI staining, and images were acquired using 20x zoom Zeiss 880 confocal microscope for morphological analysis. Each image covers a dimension of 425µm x 425µm. The cells were placed in wells with meshes coated in Collagen I after OPT treatment.*

A. Phalloidin staining of actin filaments.
B. Vinculin staining of focal adhesions.
C. DAPI staining of cell nuclei.
D. Composite image superposing Phalloidin, Vinculin, and DAPI staining to give holistic overview of control cell morphology characteristics.

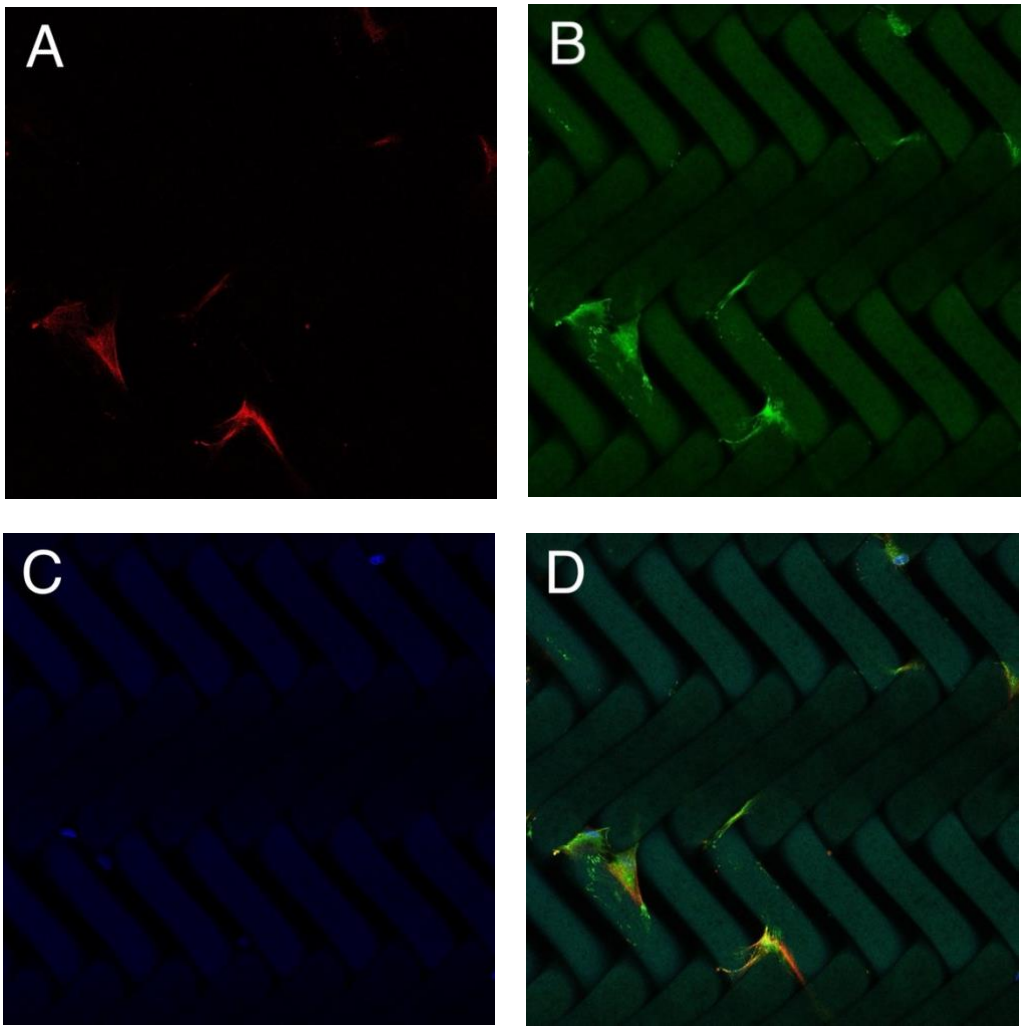

Figure 9: Confocal imaging and morphology of human osteoblast cells on a P15 peptide treated PET membrane. *Fixed cells were subjected to Vinculin, Phalloidin and DAPI staining, and images were acquired using 20x zoom Zeiss 880 confocal microscope for morphological analysis. Each image covers a dimension of 425µm x 425µm. The cells were placed in wells with meshes that underwent P15 functionalisation.*

A. Phalloidin staining of actin filaments.
B. Vinculin staining of focal adhesions.
C. DAPI staining of cell nuclei.
D. Composite image superposing Phalloidin, Vinculin, and DAPI staining to give holistic overview of control cell morphology characteristics.

By comparing figures 7-9 and complementing these representative images with those found in Appendices C.3, C.4 and C.5, several differences can be made out between the different surfaces. First, the cells that were seeded on the native samples show much weaker focal adhesion signals and are generally much smaller in size than cells in the other two meshes. This might suggest a lack of specificity from the cells to the untreated surface, which, despite being able to attach, appear to not be working under optimal conditions. This is further reinforced by the number of cells that attached to each other in the native sample compared to the number of cells that did the same in the other two samples, which proposes that the cells want to attach but may not feel comfortable enough in the native surface.

Looking at figure 8 in comparison to figure 9, it is possible to observe a greater quantity of focal adhesions for the Collagen I-coated surface over P15. The fibres in Collagen I are also

generally thicker than those of P15. This makes sense, seeing how P15 is attempting to mimic a very specific region of Collagen I, who on its own is already trying to mimic ECM-like conditions. Therefore, cells will naturally feel more comfortable, look slightly larger, and have expanded focal adhesions and thicker actin fibres.

Although they did not have the same extent of focal adhesion and specificity development as the Collagen I-coated cells, the cells seeded on the P15 surface also exhibited promising qualities. For instance, their focal adhesions are indeed larger than the native samples', as aforementioned. Moreover, taking a particular look at the bottom left corner of image D in figure 9, it is possible to see the cell "wrapping" around the fibre, with the fibre cytoskeleton showing soft signals of spreading and the presence of focal adhesion points reinforcing this idea. Additionally, P15 cells appear to be more aligned with the mesh's fibres, compared to both the Collagen I and native surfaces that appear to be more in between the fibres. This eased movement and facility to align the focal adhesions with the fibres could mean that these cells also indeed look to be comfortably attached to the P15-treated surface.

In any case, the results certainly indicate that there are differences in cell behaviour, morphology and adaptation depending on the surface that they were seeded on, with the most positive results in terms of cell requirements appearing to be on both the Collagen I and P15 treated membranes.

5. Discussion

The reduction in CA measurements at each step of the surface modification process indicates increased hydrophilicity of the PET membrane. The final substantial decrease in CA, due to peptide functionalisation, suggests the presence of highly polar or hydrophilic P15 groups on the surface, which are crucial for enhancing cell adhesion and proliferation [29]. This finding aligns with previous studies that have shown that peptide functionalisation significantly increases surface hydrophilicity and biocompatibility [27, 28]. Moreover, the application of P15 on samples that have been treated to improve hydrophilicity has been noted to display pro-osteogenic activity in previous research [31]. Together, the CA and hydrophilicity studies therefore supports the notion that this mesh functionalisation could support basic regenerative processes and suggest an applicability of this procedure as a potential means for bone regeneration.

Comparative analysis of cell behaviour on native, Collagen I-coated, and P15 functionalised surfaces reveals significant improvements in cell adhesion, morphology, and focal adhesion formation on the P15 treated surfaces. Cells on the P15 functionalised PET surface displayed larger focal adhesions than the native, and better alignment with the mesh fibres, indicative of a conducive environment for cell attachment and spreading. Therefore, the enhanced interaction between the P15 functionalised surface and bone cells supports the hypothesis that the P15 peptide enhances biocompatibility. This finding is consistent with literature reporting that peptide functionalisation significantly increases surface hydrophilicity and biocompatibility [19].

The P15 peptide could also be promoting cell attachment by developing its own "natural" ECM-like environment. This mimicking effect is critical as it encourages bone cell adhesion, proliferation, and differentiation, essential for effective bone healing and regeneration. The proposed enhanced cell attachment and proliferation that was observed on the P15 functionalised PET surface could suggest that these membranes may support the formation of

new bone tissue. In turn, this would address one of the primary challenges in non-union fracture healing, which is the inability of bone cells to proliferate and form new tissue at the fracture site [28]. The increased hydrophilicity and biocompatibility of the P15 functionalised membranes can lead to better integration with the host tissue, reducing the likelihood of immune rejection and promoting faster healing [28].

In regard to the quality of the results that were obtained, an observation can be done on the seemingly small number of cells that were found on the meshes, as more cells were expected to be present. On the 20x zoom the number of cells on the focused plane was rarely over 3, and very frequently there were areas in the mesh that had no cells at all on the focused plane. However, it must be noted that no exact number was calculated, and cell count was not noted for any samples. For a future experiment quantitative data could be integrated by taking a more methodical and less randomised approach towards confocal mesh imaging, so to be able to get an estimate on the number of cells. For this, more images would also be necessary, which would in turn imply that data collection could take a substantial amount of time.

Additionally, while it is not visible in the results above, the green vinculin staining went much better on the meshes than the red actin (phalloidin) staining, as compared to images with original contrast settings (Appendix C.2). The contrast of the phalloidin staining images had to be increased, while the vinculin's contrast had to be reduced, to best show the staining results with minimal background noise. It is possible that the dilution of vinculin with phalloidin during the immunofluorescence staining protocol may have gone wrong, so increasing the concentration of phalloidin could be a viable option for a future experiment.

6. Conclusion

All in all, the P15 peptide functionalised PET membrane mesh experiments gave a promising indication that these meshes are worth continuing investigating and may have long-term potential for clinical treatments. The promising in vitro results indicate that P15 functionalised PET membranes could potentially be applied in clinical settings in the future to support bone regeneration in non-union fractures. The application of these membranes in scaffold design, implant coatings, and hybrid constructs could revolutionise the treatment of non-union fractures, offering improved outcomes for patients.

However, to fully determine their efficacy and safety, further in vivo studies and clinical trials are necessary. These studies would assess the long-term stability, biocompatibility, and functional integration of the membranes in a living organism. Integrating P15 functionalised PET membranes into scaffold designs for bone tissue engineering could also provide structural support while enhancing cellular activities necessary for bone healing. The membranes could also be used as coatings for bone implants to improve their integration and reduce healing time by promoting better cell-surface interactions. By combining P15 functionalised PET membranes with other biocompatible materials or growth factors hybrid constructs could be created, offering synergistic benefits for bone regeneration.

7. Works Cited

[1] Wildemann, B., Ignatius, A., Leung, F. et al. Non-union bone fractures. Nature Reviews Disease Primers 7, 57 (2021). https://doi.org/10.1038/s41572-021-00289-8

[2] Andrzejowski, P., & Giannoudis, P. V. (2019). The 'diamond concept' for long bone non-union management. *Journal of orthopaedics and traumatology : official journal of the Italian Society of Orthopaedics and Traumatology*, *20*(1), 21. https://doi.org/10.1186/s10195-019-0528-0

[3] Lou, Y., Wang, H., Ye, G., Li, Y., Liu, C., Yu, M., & Ying, B. (2021). Periosteal Tissue Engineering: Current Developments and Perspectives. *Advanced healthcare materials*, *10*(12), e2100215. https://doi.org/10.1002/adhm.202100215

[4] Jiang, J., Wan, F., Yang, J., Hao, W., Wang, Y., Yao, J., Shao, Z., Zhang, P., Chen, J., Zhou, L., & Chen, S. Enhancement of osseointegration of polyethylene terephthalate artificial ligament by coating of silk fibroin and depositing of hydroxyapatite. *International journal of nanomedicine*, 9, pg. 4569–4580 (2014). https://doi.org/10.2147/IJN.S69137

[5] Sughanthy, S.A.P., Ansari, M.N.M., Atiqah, A. Dynamic mechanical analysis of polyethylene terephthalate/hydroxyapatite biocomposites for tissue engineering applications. *Journal of Materials Research and Technology*, 9, 2, pg. 2350–2356 (2020). https://doi.org/10.1016/j.jmrt.2019.12.066

[6] Czuba L. (2014). Application of Plastics in Medical Devices and Equipment. *Handbook of Polymer Applications in Medicine and Medical Devices*, 9–19. https://doi.org/10.1016/B978-0-323-22805-3.00002-5

[7] Sughanthy, S.A.P., Ansari, M.N.M., Atiqah, A. Dynamic mechanical analysis of polyethylene terephthalate/hydroxyapatite biocomposites for tissue engineering applications. Journal of Materials Research and Technology, 9, 2, pg. 2350–2356 (2020). https://doi.org/10.1016/j.jmrt.2019.12.066

[8] Gomar, F., Orozco, R., Villar, J. L., & Arrizabalaga, F. (2007). P-15 small peptide bone graft substitute in the treatment of non-unions and delayed union. A pilot clinical trial. *International orthopaedics*, *31*(1), 93–99. https://doi.org/10.1007/s00264-006-0087-x

[9] *Cell Culture Inserts - US*. (n.d.). Www.thermofisher.com. Retrieved May 24, 2024, from https://www.thermofisher.com/nl/en/home/life-science/cell-culture/cell-culture-plastics/cell-culture-inserts.html?CID=fl-cellcultureinserts

[10] Hennessy, K. M., Pollot, B. E., Clem, W. C., Phipps, M. C., Sawyer, A. A., Culpepper, B. K., & Bellis, S. L. (2009). The effect of collagen I mimetic peptides on mesenchymal stem cell adhesion and differentiation, and on bone formation at hydroxyapatite surfaces. *Biomaterials*, *30*(10), 1898–1909. https://doi.org/10.1016/j.biomaterials.2008.12.053

[11] *Sulfo-NHS (N-hydroxysulfosuccinimide)*. (n.d.). Www.thermofisher.com. https://www.thermofisher.com/document-connect/document-connect.html?url=https://assets.thermofisher.com/TFS-Assets%2FLSG%2Fmanuals%2FMAN0011309_NHS_SulfoNHS_UG.pdf

[12] Zhao, X., Zhuang, Y., Cao, Y., Cai, F., Yicheng Lv, Zheng, Y., Yang, J., & Shi, X. (2024). Electrospun Biomimetic Periosteum Capable of Controlled Release of Multiple Agents for Programmed Promoting Bone Regeneration. *Advanced Healthcare Materials*, *13*(12). https://doi.org/10.1002/adhm.202303134

[13] Bhatnagar, R. S., Shattuck, M. B., Jing Jing Qian, Gough, C. A., & Nicoll, S. B. (2000). Theoretical and Experimental Approaches to Identification of a Fiber Surface Cell Binding Domain in Collagen and its Application in Tissue Engineering. *Microscopy and Microanalysis*, *6*(S2), 986–987. https://doi.org/10.1017/s1431927600037429

[14] Martinez Serrano, A., BSc. Thesis (2023), University of Twente, Title: PEPTIDE-FUNCTIONALIZED MEMBRANE IN ORGAN-ON-CHIP MODEL TO ENHANCE BONE HEALING

[15] Lin, Z., Solomon, K. L., Zhang, X., Pavlos, N. J., Abel, T., Willers, C., Dai, K., Xu, J., Zheng, Q., & Zheng, M. (2011). In vitro evaluation of natural marine sponge collagen as a scaffold for bone tissue engineering. *International journal of biological sciences*, *7*(7), 968–977. https://doi.org/10.7150/ijbs.7.968

[16] Dimitriou, R., Jones, E., McGonagle, D., & Giannoudis, P. V. (2011). Bone regeneration: current concepts and future directions. *BMC medicine*, *9*, 66. https://doi.org/10.1186/1741-7015-9-66

[17] Perez, J. R., Kouroupis, D., Li, D. J., Best, T. M., Kaplan, L., & Correa, D. (2018). Tissue Engineering and Cell-Based Therapies for Fractures and Bone Defects. *Frontiers in bioengineering and biotechnology*, *6*, 105. https://doi.org/10.3389/fbioe.2018.00105

[18] Collier, J. H., & Segura, T. (2011). Evolving the use of peptides as components of biomaterials. *Biomaterials*, *32*(18), 4198–4204. https://doi.org/10.1016/j.biomaterials.2011.02.030

[19] Allen, M. R., Hock, J. M., & Burr, D. B. (2004). Periosteum: biology, regulation, and response to osteoporosis therapies. *Bone*, *35*(5), 1003–1012. https://doi.org/10.1016/j.bone.2004.07.014

[20] Liu, Q., Limthongkul, W., Sidhu, G., Zhang, J., Vaccaro, A., Shenck, R., Hickok, N., Shapiro, I., & Freeman, T. (2012). Covalent attachment of P15 peptide to titanium surfaces enhances cell attachment, spreading, and osteogenic gene expression. *Journal of Orthopaedic Research*, *30*(10), 1626–1633. https://doi.org/10.1002/jor.22116

[21] Jafari, M., Paknejad, Z., Rad, M. R., Motamedian, S. R., Eghbal, M. J., Nadjmi, N., & Khojasteh, A. (2015). Polymeric scaffolds in tissue engineering: a literature review. *Journal of Biomedical Materials Research Part B: Applied Biomaterials*, *105*(2), 431–459. https://doi.org/10.1002/jbm.b.33547

[22] Wang, Y., Wang, X., Lu, W., Yuan, Q., Zheng, Y., & Yao, B. (2019). A thin film polyethylene terephthalate (PET) electrochemical sensor for detection of glucose in sweat. *Talanta*, *198*, 86–92. https://doi.org/10.1016/j.talanta.2019.01.104

[23] Lu, H., Hoshiba, T., Kawazoe, N., Koda, I., Song, M., & Chen, G. (2011). Cultured cell-derived extracellular matrix scaffolds for tissue engineering. *Biomaterials*, *32*(36), 9658–9666. https://doi.org/10.1016/j.biomaterials.2011.08.091

[24] Humphries, J. D., Byron, A., & Humphries, M. J. (2006). Integrin ligands at a glance. *Journal of cell science*, *119*(Pt 19), 3901–3903. https://doi.org/10.1242/jcs.03098

[25] Wulf, E., Deboben, A., Bautz, F. A., Faulstich, H., & Wieland, T. (1979). Fluorescent phallotoxin, a tool for the visualization of cellular actin. *Proceedings of the National Academy of Sciences of the United States of America*, *76*(9), 4498–4502. https://doi.org/10.1073/pnas.76.9.4498

[26] Kapuscinski J. (1995). DAPI: a DNA-specific fluorescent probe. *Biotechnic & histochemistry : official publication of the Biological Stain Commission*, *70*(5), 220–233. https://doi.org/10.3109/10520299509108199

[27] Gotoh, K., Yasukawa, A. & Kobayashi, Y. Wettability characteristics of poly(ethylene terephthalate) films treated by atmospheric pressure plasma and ultraviolet excimer light. *Polymer Journal*, 43, pg. 545–551 (2011). https://doi.org/10.1038/pj.2011.20

[28] Vasilieva, T., Nikolskaya, E., Vasiliev, M., Mollaeva, M., Chirkina, M., Sokol, M., Yabbarov, N., Shikova, T., Abramov, A., & Ugryumov, A. (2024). Applicability of Electron-Beam and Hybrid Plasmas for Polyethylene Terephthalate Processing to Obtain Hydrophilic and Biocompatible Surfaces. *Polymers*, *16*(2), 172. https://doi.org/10.3390/polym16020172

[29] Kuddannaya, S., Chuah, Y. J., Lee, M. H. A., Menon, N. V., Kang, Y., & Zhang, Y. (2013). Surface Chemical Modification of Poly(dimethylsiloxane) for the Enhanced Adhesion and Proliferation of Mesenchymal Stem Cells. *ACS Applied Materials & Interfaces*, *5*(19), 9777–9784. https://doi.org/10.1021/am402903e

[30] Fischer, M. J. E. (2010). Amine Coupling Through EDC/NHS: A Practical Approach. *Methods in Molecular Biology*, *627*, 55–73. https://doi.org/10.1007/978-1-60761-670-2_3

[31] Li, X., Contreras-Garcia, A., LoVetri, K., Yakandawala, N., Wertheimer, M. R., De Crescenzo, G., & Hoemann, C. D. (2015). Fusion peptide P15-CSP shows antibiofilm activity and pro-osteogenic activity when deposited as a coating on hydrophilic but not hydrophobic surfaces. *Journal of biomedical materials research. Part A*, *103*(12), 3736–3746. https://doi.org/10.1002/jbm.a.35511

[32] Kyte, J., & Doolittle, R. F. (1982). A simple method for displaying the hydropathic character of a protein. *Journal of Molecular Biology*, *157*(1), 105–132. https://doi.org/10.1016/0022-2836(82)90515-0

[33] Aysegul Dede Eren, Amy, Urandelger Tuvshindorj, Truckenmüller, R., Giselbrecht, S., E. Deniz Eren, Mehmet Orhan Tas, Phanikrishna Sudarsanam, & Jan de Boer. (2022). Cells Dynamically Adapt to Surface Geometry by Remodeling Their Focal Adhesions and Actin Cytoskeleton. *Frontiers in Cell and Developmental Biology*, *10*. https://doi.org/10.3389/fcell.2022.863721

[34] Legerstee, K., & Houtsmuller, A. (2021). A Layered View on Focal Adhesions. *Biology*, *10*(11), 1189. https://doi.org/10.3390/biology10111189

[35] Pasman, T., Baptista, D., van Riet, S., Truckenmüller, R. K., Hiemstra, P. S., Rottier, R. J., Hamelmann, N. M., Paulusse, J. M. J., Stamatialis, D., & Poot, A. A. (2021). Development of an In Vitro Airway Epithelial–Endothelial Cell Culture Model on a Flexible Porous Poly(Trimethylene Carbonate) Membrane Based on Calu-3 Airway Epithelial Cells and Lung

Microvascular Endothelial Cells. *Membranes*, *11*(3), 197. https://doi.org/10.3390/membranes11030197

[36] *Fix, Perm, & Block - US*. (n.d.). Www.thermofisher.com. Retrieved June 26, 2024, from https://www.thermofisher.com/nl/en/home/life-science/cell-analysis/cell-analysis-learning-center/molecular-probes-school-of-fluorescence/imaging-basics/protocols-troubleshooting/protocols/fix-perm-block.html

[37] Im, K., Mareninov, S., Diaz, M. F. P., & Yong, W. H. (2019). An introduction to Performing Immunofluorescence Staining. *Methods in Molecular Biology (Clifton, N.J.)*, *1897*(2), 299–311. https://doi.org/10.1007/978-1-4939-8935-5_26

[38] Koçer, G., Albino, I. M. C., Verheijden, M. L., & Jonkheijm, P. (2022). Endothelial cell spreading on lipid bilayers with combined integrin and cadherin binding ligands. *Bioorganic & Medicinal Chemistry*, *68*, 116850. https://doi.org/10.1016/j.bmc.2022.116850

Appendix A: Contextual Exploration

A.1 Contextual applicability and result usefulness

Worldwide, 5% of the population suffer from non-union bone fractures, which is associated with debilitating pain, loss of function and psychosocial disability in patients, significantly decreasing the quality of life [1]. Therefore, tissue regeneration and biomaterials strategies are now focusing on the development of sustainable solutions to increase the speed and quality of bone healing. This BSc project is part of a larger consortium project between material chemists and biomedical engineers at the University of Twente and biologists and clinicians from Vrije Universiteit Amsterdam. It will contribute to the initial steps to convert a clinically applied, mechanically robust, but biologically inert material into a new multi(bio)functional biomaterial with periosteum-like cell-adhesive and cell-instructive properties. The final multi(bio)functional biomaterial has a high clinical potential for bone healing. This new biomaterial system will present an unmatched precise control over presented biofunctional properties, owing to its fully synthetic and user-defined nature.

While this BSc project focuses on the interactions between the biomaterial and bone cells, in the future, the fully functional (final) biomaterial is envisioned to also support cells involved in pro-regenerative responses and blood vessel formation. Following a proof-of-principle and performance evaluation, further development and preclinical validation of a new bone-lining graft biomaterial is expected.

Besides using this new biomaterial system (together with its implementation into near-physiological bone-on-chip platform), we will improve our understanding on the healing potential of primary human bone tissue/cells in synergy with supportive (pro-regenerative) cells, in response to biofunctional factors guided by our periosteum-mimetic biomaterial, in an unprecedented way. By incorporation of human-derived bone tissue fragments from different donors into our experimental design, we will be able to achieve a more personalised insight in cell and tissue behaviour. This will pave the way for tailor-made biomaterial-based solutions for patients. In the future, we expect that our platform will not only serve for bone tissue engineering, but also for bone tissue therapy as well as will complement preclinical research and offer reduction of animals in biomaterials research.

When successfully validated, our envisioned clinically relevant biomaterial is set to enhance the healing potential of non-unions and the speed of recovery, saving significant time and

resources while tackling this clinical problem as well as significantly contribute to improve patients' quality of life.

A.2 Limitations

Firstly, the reliance on simplified in vitro models, such as cell culture systems and bone-on-chip devices, may not fully capture the complexity of the in vivo bone microenvironment. This discrepancy between in vitro and in vivo conditions could potentially limit the translational relevance of the findings and their applicability in clinical settings. Moreover, despite efforts to mimic aspects of the periosteum and facilitate bone healing, the biological complexity of the processes involved remains a significant challenge. While the project aims to replicate certain properties of native tissue, achieving a comprehensive understanding and faithful replication of the periosteum's functions may prove challenging given its multifaceted nature.

Additionally, concerns regarding biomaterials biocompatibility and long-term safety pose significant challenges. Despite advancements in biomaterials design, there remains a risk of adverse reactions or immune responses to the implanted materials, which could hinder their clinical utility and acceptance.

Furthermore, transitioning from laboratory-scale research to clinical applications presents formidable obstacles. Regulatory approval, scalability, and cost-effectiveness are crucial considerations that must be addressed to ensure successful clinical translation of the developed biomaterials and therapies. The complexity of the bone healing cascade adds another layer of challenge. While the project focuses on specific aspects such as cell adhesion, proliferation, and differentiation, bone regeneration involves a myriad of factors, including growth factors, cytokines, and mechanical stimuli. Capturing this complexity in experimental setups is inherently difficult.

Ethical and regulatory considerations surrounding the use of human-derived cells and materials, as well as the regulatory requirements for biomedical research, impose additional constraints on the project's scope and implementation. Balancing ethical considerations with scientific objectives is essential for conducting responsible and impactful research.

Finally, resource and time constraints may limit the scope and pace of research progress. Adequate funding, equipment, and personnel are essential for conducting robust experiments and data analysis. Managing these resources effectively while maintaining research quality is crucial for the project's success.

A.3 Interdisciplinarity of the project

This project epitomises interdisciplinary collaboration, bringing together expertise from various fields to tackle the multifaceted challenge of non-union bone fractures.

Biomaterials engineering and material science play pivotal roles in the project. Researchers leverage biomaterials engineering principles to develop synthetic membranes that mimic the periosteum, drawing upon knowledge of material properties and fabrication techniques. Materials science expertise guides the selection of materials with appropriate mechanical properties, such as polyethylene terephthalate (PET), ensuring the efficacy of the developed membranes.

Cell biology and biochemistry are also integral to understanding cellular behaviour on biomaterial surfaces. Insights from cell biology elucidate the intricate processes of cell

adhesion, proliferation, differentiation, and signalling, providing crucial information for optimising biomaterial-cell interactions. Biochemical expertise drives the design of peptides that promote cell adhesion and facilitate the delivery of bioactive factors like BMP-2 to cells, enhancing the regenerative potential of the biomaterials.

Regenerative medicine and tissue engineering principles guide the project towards developing biomaterials that promote natural bone healing processes. By aligning with the principles of regenerative medicine, the project aims to create periosteum-mimetic grafts that facilitate bone regeneration, offering innovative solutions for addressing non-union bone fractures.

Collaboration with clinicians underscores the project's focus on clinical translation and biomedical applications. Clinician input ensures that the developed biomaterials meet clinical needs and can be seamlessly integrated into practical applications. Understanding the biological processes underlying non-union bone fractures is essential for developing innovative clinical treatments that enhance patient outcomes.

The project also encompasses elements of biophysics and microfluidics. Biophysical techniques are employed to characterise the physical properties of biomaterials, providing insights into surface modifications and material behaviour. Utilising bone-on-chip microfluidic devices enables researchers to study tissue responses under controlled conditions, leveraging principles from microfluidics and organ-on-a-chip technologies.

Through interdisciplinary collaboration and integration of diverse expertise, the project endeavours to develop innovative solutions for non-union bone fractures, highlighting the critical role of interdisciplinary approaches in advancing biomedical research and healthcare.

Appendix B: Reaction Mechanism

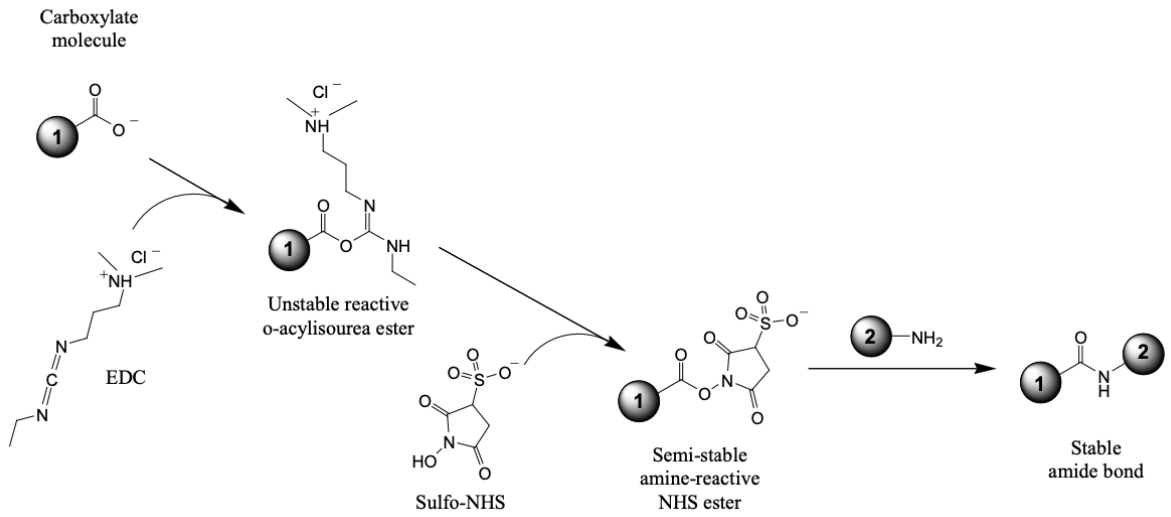

Figure 10: *Reaction mechanism of EDC-mediated NHS reaction between PET surface and P15, which would replace molecules 1 and 2 [11].*

Appendix C: Additional Immunofluorescence Imaging Results

Additional images were taken of the meshes that received different treatments. These images were used to best analyse and aid in the ultimate selection of a representative image, like the one that was used in the results section. Below, some other relevant images used in the process.

C.1 Immunofluorescence of Collagen I and FBS-Coated Cells

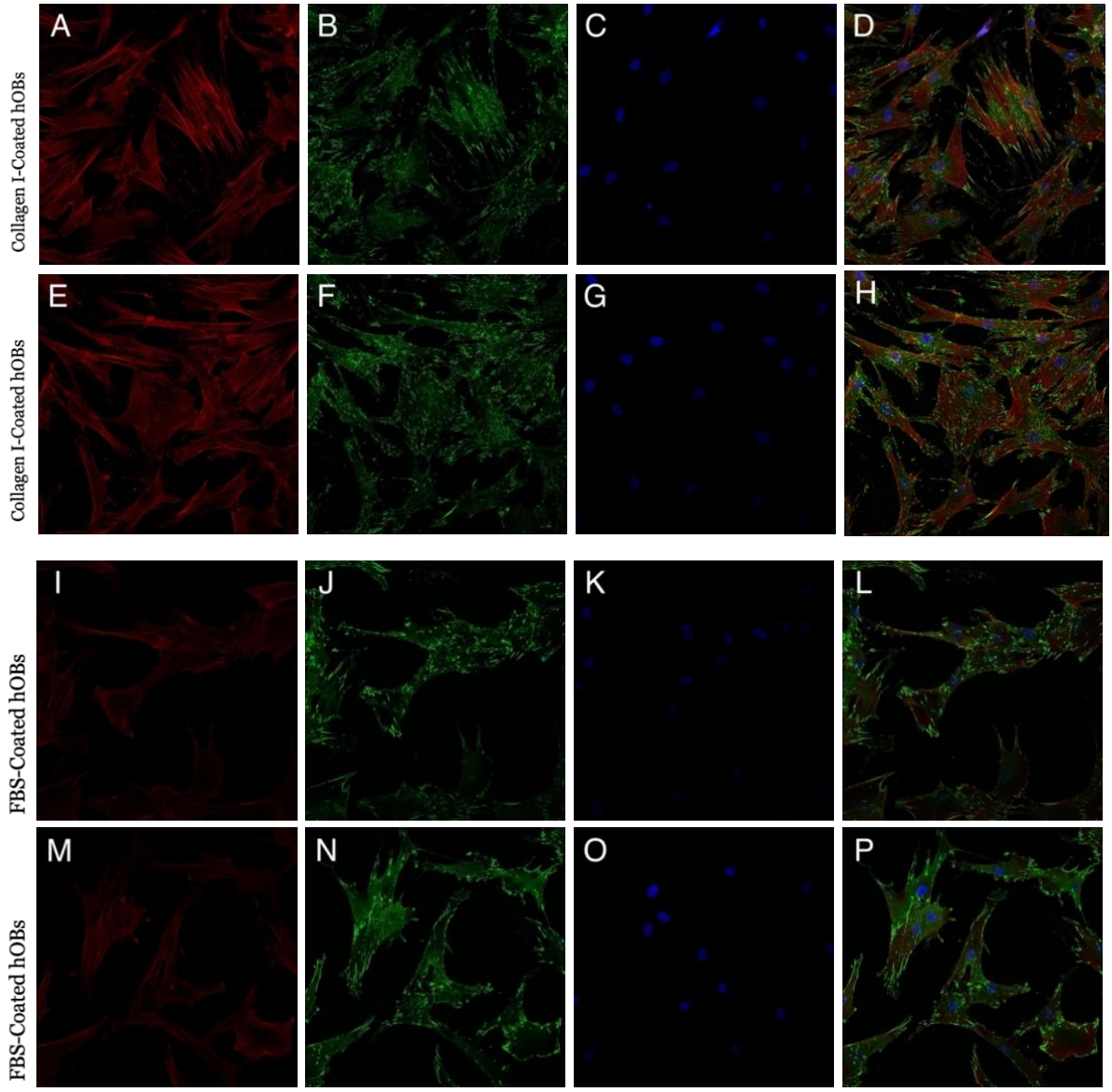

Figure 11: Confocal images and morphology of Collagen I and FBS-coated human osteoblast cells. *Fixed cells were subjected to Vinculin, Phalloidin and DAPI staining, and images were acquired using 20x zoom Zeiss 880 confocal microscope for morphological analysis. Each image covers a dimension of 425µm x 425µm. The cells were seeded in 6 wells of a 96 well glass plate coated in either Collagen I or FBS.*

A–D. Image 1 of Collagen I-coated hOBs. Phalloidin staining of actin filaments; vinculin staining of focal adhesions; DAPI staining of cell nuclei; Composite images superposing all stainings to give holistic overview of control cell morphology characteristics.
E–H. Image 2 of Collagen I-coated hOBs. (E) Phalloidin staining of actin filaments; (F) vinculin staining of focal adhesions; (G) DAPI staining of cell nuclei; (H) Composite image superposing all stainings to give holistic overview of control cell morphology characteristics.

I–L. Image 1 of FBS-coated hOBs. (I) Phalloidin staining of actin filaments; (J) vinculin staining of focal adhesions; (K) DAPI staining of cell nuclei; (L) Composite image superposing all stainings to give holistic overview of control cell morphology characteristics.
M-P. Image 2 of FBS-coated hOBs. (M) Phalloidin staining of actin filaments; (N) vinculin staining of focal adhesions; (O) DAPI staining of cell nuclei; (P) Composite image superposing all stainings to give holistic overview of control cell morphology characteristics.

C.2 Original (Unedited) Confocal Images Used in Results

Images showing immunofluorescence of hOBs on Native, Collagen I-Coated, and P15 Treated meshes prior to editing for improved contrast and staining results.

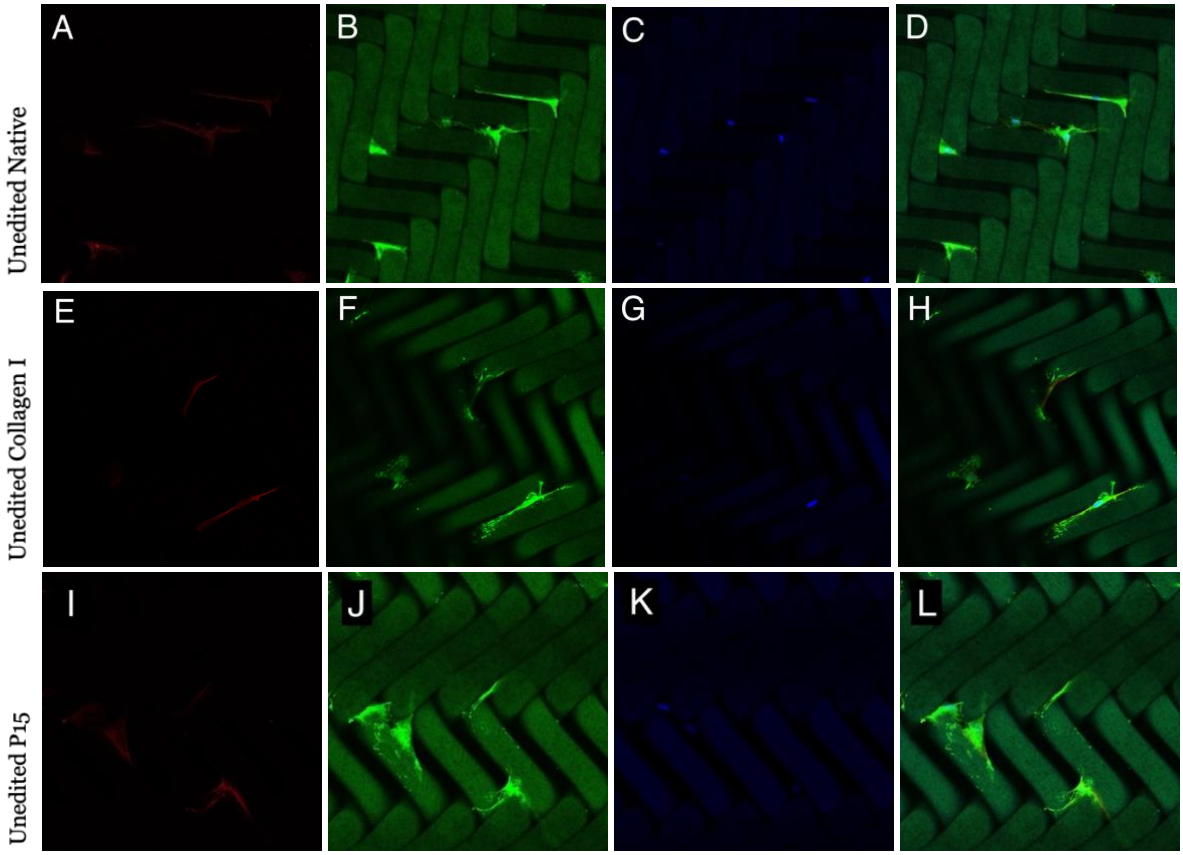

Figure 12: Confocal imaging and morphology of human osteoblast cells on two different sections of Native PET membrane. *Fixed cells were subjected to Vinculin, Phalloidin and DAPI staining, and images were acquired using 20x zoom Zeiss 880 confocal microscope for morphological analysis. Each image covers a dimension of 425µm x 425µm. The cells were placed in wells with untreated meshes.*

A-D. Unedited version of image used in Figure 7, showing hOBs on Native PET mesh. (A) Phalloidin staining of actin filaments; (B) vinculin staining of focal adhesions; (C) DAPI staining of cell nuclei; (D) Composite image superposing all stainings to give holistic overview of control cell morphology characteristics.
E-H. Unedited version of image used in Figure 8, showing hOBs on Collagen I-coated PET mesh. (E) Phalloidin staining of actin filaments; (F) vinculin staining of focal adhesions; (G) DAPI staining of cell nuclei; (H) Composite image superposing all stainings to give holistic overview of control cell morphology characteristics.
I-L. Unedited version of image used in Figure 9, showing hOBs on P15-treated PET mesh. (E) Phalloidin staining of actin filaments; (F) vinculin staining of focal adhesions; (G) DAPI staining of cell nuclei; (H) Composite image superposing all stainings to give holistic overview of control cell morphology characteristics.

C.3 Immunofluorescence of Native Meshes

Comparison of two images of hOBs on native meshes after applying the same contrast editing to improve cell staining visibility and reduce background noise.

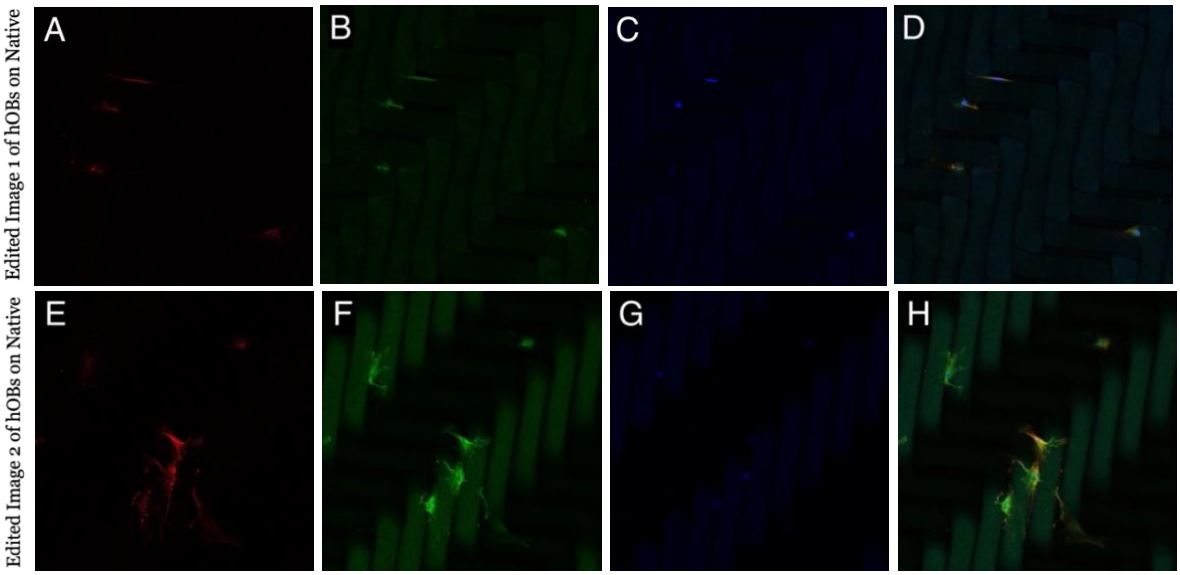

Figure 13: Confocal imaging and morphology of human osteoblast cells on two different sections of Native PET membrane. *Fixed cells were subjected to Vinculin, Phalloidin and DAPI staining, and images were acquired using 20x zoom Zeiss 880 confocal microscope for morphological analysis. Each image covers a dimension of 425µm x 425µm. The cells were placed in wells with untreated meshes. These images are examples of the data that was used as a basis of comparison and generalisation of the results, to ultimately select and include the most "representative" image.*

A-D. Edited image 1 of hOBs on a random Native PET mesh area to match contrast settings of images used in Figure 8 of results section. (A) Phalloidin staining of actin filaments; (B) vinculin staining of focal adhesions; (C) DAPI staining of cell nuclei; (D) Composite image superposing all stainings to give holistic overview of control cell morphology characteristics.
E-H. Edited image 2 of hOBs on another random Native PET mesh area to match contrast settings of images used in Figures 8 of results section. (E) Phalloidin staining of actin filaments; (F) vinculin staining of focal adhesions; (G) DAPI staining of cell nuclei; (H) Composite image superposing all stainings to give holistic overview of control cell morphology characteristics.

C.4 Immunofluorescence of Collagen I and OPT+PBS Coated Meshes

Comparison of two different images of hOBs on Collagen I-coated meshes after applying the same contrast editing to improve cell staining visibility and reduce background noise.

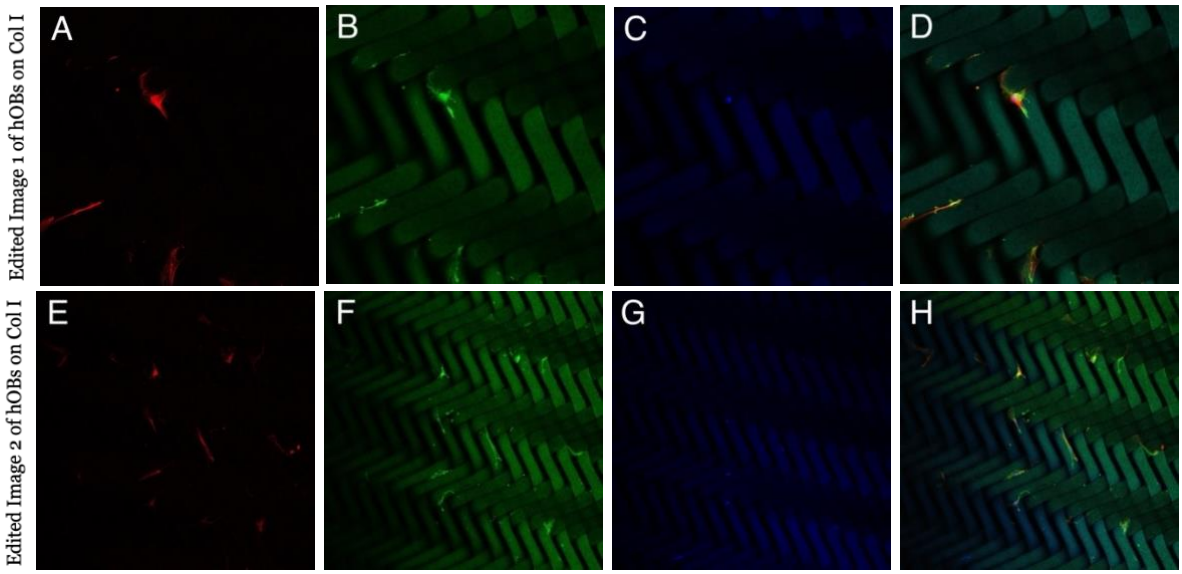

Figure 14: Confocal imaging and morphology of human osteoblast cells on two different sections of Collagen I-coated PET membrane. *Fixed cells were subjected to Vinculin, Phalloidin and DAPI staining, and images were acquired using 20x and 10x zoom Zeiss 880 confocal microscope for morphological analysis. Each image covers a dimension of 425µm x 425µm. The cells were placed in wells with untreated meshes. These images are examples of the data that was used as a basis of comparison and generalisation of the results, to ultimately select and include the most "representative" image.*

A-D. Edited image 1 of hOBs on a random Collagen I-coated PET mesh area to match contrast settings of images used in Figure 8 of results section, taken with 20x zoom. (A) Phalloidin staining of actin filaments; (B) vinculin staining of focal adhesions; (C) DAPI staining of cell nuclei; (D) Composite image superposing all stainings to give holistic overview of control cell morphology characteristics.
E-H. Edited image 2 of hOBs on another random Collagen I-coated PET mesh area to match contrast settings of images used in Figure 8 of results section, taken with 10x zoom. (E) Phalloidin staining of actin filaments; (F) vinculin staining of focal adhesions; (G) DAPI staining of cell nuclei; (H) Composite image superposing all stainings to give holistic overview of control cell morphology characteristics.

C.5 Immunofluorescence of P15 Peptide-Treated Meshes

Comparison of two different images of hOBs on P15-treated meshes after applying the same contrast editing to improve cell staining visibility and reduce background noise.

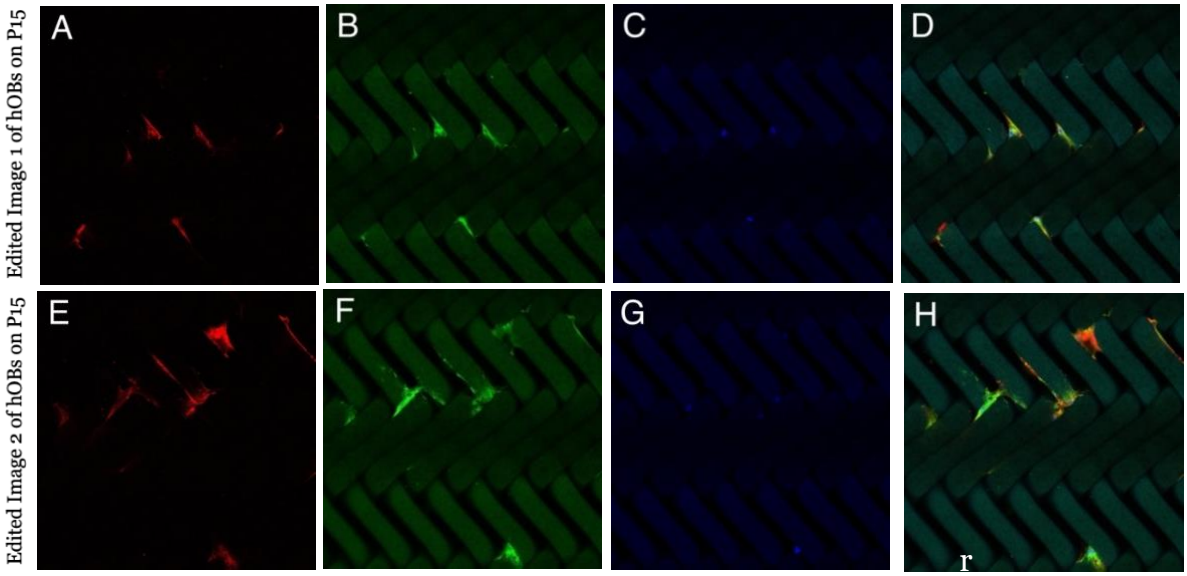

Figure 15: Confocal imaging and morphology of human osteoblast cells on two different sections of P15-treated PET membrane. *Fixed cells were subjected to Vinculin, Phalloidin and DAPI staining, and images were acquired using 20x zoom Zeiss 880 confocal microscope for morphological analysis. Each image covers a dimension of 425µm x 425µm. The cells were placed in wells with untreated meshes. These images are examples of the data that was used as a basis of comparison and generalisation of the results, to ultimately select and include the most "representative" image.*

A-D. Edited image 1 of hOBs on a random P15-treated PET mesh area to match contrast settings of images used in Figure 9 of results section. (A) Phalloidin staining of actin filaments; (B) vinculin staining of focal adhesions; (C) DAPI staining of cell nuclei; (D) Composite image superposing all stainings to give holistic overview of control cell morphology characteristics.
E-H. Edited image 2 of hOBs on another random P15-treated PET mesh section to match contrast settings of images used in Figure 9 of results section. (E) Phalloidin staining of actin filaments; (F) vinculin staining of focal adhesions; (G) DAPI staining of cell nuclei; (H) Composite image superposing all stainings to give holistic overview of control cell morphology characteristics.

Appendix D: HOBs in Cell Culture Brightfield Microscopy Imaging

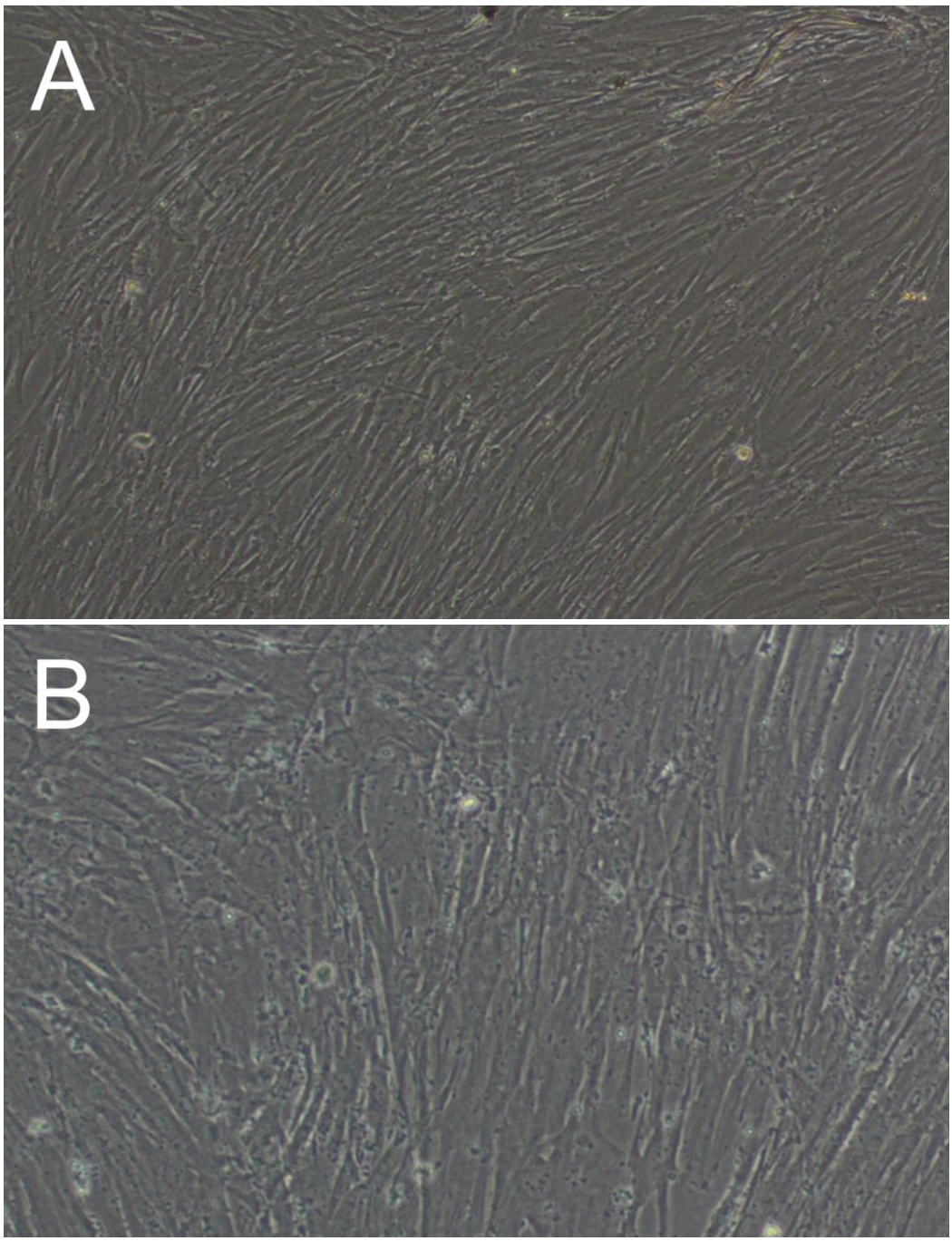

Figure 16: Brightfield microscopy imaging of human osteoblast cells prior to transfer to meshes. *The cells were cultured in medium with serum (αMEM + 10% FBS + 1% P/S). The images were taken in day 7 after being passaged for a third time. They were then passaged one last time when being transferred onto serum-less medium with meshes.*

A. Brightfield image taken with 4x zoom of hOB cells in medium with serum.
B. Brightfield image taken with 10x zoom of hOB cells in medium with serum.